

Three-dimensional Structure of a Kunitz-type Inhibitor in Complex with an Elastase-like Enzyme*

Received for publication, February 25, 2015, and in revised form, April 7, 2015. Published, JBC Papers in Press, April 15, 2015, DOI 10.1074/jbc.M115.647586

Rossana García-Fernández[‡], Markus Perbandt^{§¶}, Dirk Rehders^{||}, Patrick Ziegelmüller[§], Nicolas Piganeau[§], Ulrich Hahn[§], Christian Betzel[§], María de los Ángeles Chávez[‡], and Lars Redecke^{||1}

From the [‡]Centro de Estudio de Proteínas, Facultad de Biología, Universidad de la Habana, 20146 Habana, Cuba, the [§]Institute of Biochemistry and Molecular Biology, Department of Chemistry, University of Hamburg, 22761 Hamburg, Germany, the [¶]Hamburg Centre for Ultrafast Imaging, 22761 Hamburg, Germany, and the ^{||}Joint Laboratory for Structural Biology of Infection and Inflammation, Institute of Biochemistry and Molecular Biology, University of Hamburg, 20146 Hamburg, Germany, and Institute of Biochemistry, University of Lübeck, c/o Deutsches Elektronen Synchrotron (DESY), 22603 Hamburg, Germany

Background: Kunitz-type inhibitors provide a suitable scaffold for novel elastase inhibitors.

Results: The inhibitor ShPI-1 was modified for pancreatic elastase binding, and the crystal structure of the complex was elucidated and analyzed.

Conclusion: The extended protease-inhibitor interactions provide a potential switch to direct inhibitor selectivity toward elastases.

Significance: These results will help to design novel elastase inhibitors for the treatment of tissue destruction diseases.

Elastase-like enzymes are involved in important diseases such as acute pancreatitis, chronic inflammatory lung diseases, and cancer. Structural insights into their interaction with specific inhibitors will contribute to the development of novel anti-elastase compounds that resist rapid oxidation and proteolysis. Proteinaceous Kunitz-type inhibitors homologous to the bovine pancreatic trypsin inhibitor (BPTI) provide a suitable scaffold, but the structural aspects of their interaction with elastase-like enzymes have not been elucidated. Here, we increased the selectivity of ShPI-1, a versatile serine protease inhibitor from the sea anemone *Stichodactyla helianthus* with high biomedical and biotechnological potential, toward elastase-like enzymes by substitution of the P1 residue (Lys¹³) with leucine. The variant (rShPI-1/K13L) exhibits a novel anti-porcine pancreatic elastase (PPE) activity together with a significantly improved inhibition of human neutrophil elastase and chymotrypsin. The crystal structure of the PPE-rShPI-1/K13L complex determined at 2.0 Å resolution provided the first details of the canonical interaction between a BPTI-Kunitz-type domain and elastase-like enzymes. In addition to the essential impact of the variant P1 residue for complex stability, the interface is improved by increased contributions of the primary and secondary binding loop as compared with similar trypsin and chymotrypsin complexes. A comparison of the interaction network with elastase

complexes of canonical inhibitors from the chelonian in family supports a key role of the P3 site in ShPI-1 in directing its selectivity against pancreatic and neutrophil elastases. Our results provide the structural basis for site-specific mutagenesis to further improve the binding affinity and/or direct the selectivity of BPTI-Kunitz-type inhibitors toward elastase-like enzymes.

Elastases represent highly specific serine proteases that catalyze the cleavage of fibrous elastin, a connective tissue protein that causes tissue shape reconstruction after stretching and contradiction, as well as other extracellular matrix proteins (1). Elastin is particularly abundant in the lungs but is also present in arteries, skin, and ligaments. Consequently, abnormal elastolytic activities are considered to play important roles in tissue destruction associated with several diseases (2–5, 7–10). Under normal physiological conditions, human neutrophil elastase (HNE)² is tightly controlled by its endogenous inhibitors. However, their HNE affinity is strongly decreased by oxidative stress and by proteases released from leukocytes that are recruited to inflammation sites (5). Synthetic elastase inhibitors have been tested without satisfactory results (3, 7), highlighting the need to identify or to develop novel anti-elastase molecules that resist rapid oxidation and proteolysis to control elastase-associated diseases.

The molecular mechanisms of HNE activity are well understood, but structural data on its specific inhibition by other proteins are limited, largely because of protein glycosylation and release of a series of isoenzymes (11). Solely HNE complexes with two canonical inhibitors, the C-terminal domain of SLPI (1/2SLPI) (12) and the Kazal-type inhibitor OMTKY3 (13), have been reported. For the natively non-glycosylated porcine pancreatic elastase (PPE), x-ray structures have been

* This work was supported by Grants F4086-1 and F4086-2 from the International Foundation for Science, Sweden; the German Academic Exchange Service (DAAD); the excellence cluster (The Hamburg Centre for Ultrafast Imaging-Structure, Dynamics, and Control of Matter at the Atomic Scale) of the Deutsche Forschungsgemeinschaft; and Grant 01DN13028 from the German Federal Ministry of Education and Research.

The atomic coordinates and structure factors (code 3UOU) have been deposited in the Protein Data Bank (<http://www.pdb.org/>).

¹ To whom correspondence should be addressed: Joint Laboratory for Structural Biology of Infection and Inflammation, Inst. of Biochemistry and Molecular Biology, University of Hamburg, and Inst. of Biochemistry, University of Lübeck, c/o DESY, Bldg. 22a, Notkestr. 85, 22603 Hamburg, Germany. Tel.: 49-40-8998-5389; Fax: 49-40-8998-4747; E-mail: redecke@biochem.uni-luebeck.de.

² The abbreviations used are: HNE, human neutrophil elastase; BPTI, bovine pancreatic trypsin inhibitor; PDB, protein data bank; pNA, p-nitroanilide; PPE, porcine pancreatic elastase; ShPI-1, *Stichodactyla helianthus* protease inhibitor 1; WAP, wheat acidic protein.

solved in complex with three canonical inhibitors, namely elafin from the chelonian family (14), the *Ascaris*-type inhibitor C/E-1 (15), and a hybrid molecule (HEI-TOE) in which the binding loop of the squash-type inhibitor from *Ecballium elaterium* was substituted by a sequence derived from the third domain of the Kazal-type turkey ovomucoid inhibitor (16).

Among the canonical inhibitors of serine proteases, the BPTI-Kunitz family (PFAM PF00014) represents one of the most studied, particularly its prototypical member BPTI (17–19). BPTI-Kunitz inhibitors usually contain a basic residue at the reactive site, denoted as P1 position by Schechter and Berger (20). Thus, they strongly inhibit trypsin-like enzymes, but also chymotrypsin and HNE, with comparatively lower affinity. In contrast, the interaction with PPE is usually very weak or not observed at all (18, 21). This elastase specificity could be attributed to a more flexible S1 pocket in HNE that allows accommodation of a broad variety of P1 residues (11, 22–24). Supporting this concept, the substitution at P1 position with amino acids characterized by medium-sized hydrophobic side chains, such as Val, Ala, and Leu, not only increases the affinity of BPTI for HNE (25–27) but also converts it into a tight-binding inhibitor of pancreatic elastase with K_i values around 10^{-9} M. Affinity selection of a phage-displayed library of BPTI variants against PPE reveals an almost exclusive preference for Leu at the P1 position (28). Selectivity toward HNE or PPE is also described for other canonical inhibitor families, additionally indicating the importance of further subsites other than P1 for the elastase interaction (12).

The stability and experimental tractability of BPTI-Kunitz-type inhibitors have favored their exploration among canonical inhibitors as a scaffold for the development of protein therapeutics targeting different serine proteases (29–31). Although the structural details of trypsin and chymotrypsin inhibition by BPTI have been extensively investigated (32–35), the structural basis of the elastase specificity has not been elucidated for this type of inhibitors. Together with the large number of available mutagenesis studies (25–28), structural insights into the elastase interaction could provide important information for the design of novel potent elastase inhibitors exploiting the Kunitz-type scaffold.

We reported previously the isolation as well as functional and structural characterization of the BPTI-Kunitz-type inhibitor ShPI-1 from the Caribbean sea anemone *Stichodactyla helianthus* (UniProt accession number P31713) (21, 36). This molecule inhibits not only serine proteases but also cysteine and aspartic proteases such as papain and pepsin with K_i values in the nanomolar range (21), qualifying ShPI-1 for biotechnological use (37). We recently presented the three-dimensional structure of free and trypsin-bound recombinant ShPI-1 (*rShPI-1A*) (35, 38), revealing a high degree of conservation for the intermolecular interactions around the basic P1 residue (Lys¹³) compared with homologous complexes of mammalian inhibitors. However, a prominent stabilizing role of arginine at the P3 position was identified as the most significant deviation, thus far unique within this inhibitor family.

Obtaining new variants of ShPI-1 will increase its biomedical and biotechnological capabilities. Thus, we report here its transformation into a specific pancreatic elastase inhibitor. Although the site-directed K13L replacement also maintains

the inhibitory activity against chymotrypsin and HNE, trypsin inhibition is significantly reduced. The crystal structure of *rShPI-1/K13L* in complex with PPE determined at 2.0 Å resolution allowed the detailed investigation of the first example of a BPTI-Kunitz inhibitor/elastase interaction. Compared with the trypsin and chymotrypsin complexes of *rShPI-1A*, the interface with PPE is improved by increased contributions of the primary inhibitor binding loop and of glycine residues close to the secondary binding loop. A comparison with other canonical inhibitors in complex with HNE and PPE revealed that the side chain of Arg¹¹ at the P3 site of ShPI-1/K13L extends into the same enzyme region as the P5 residue of chelonians, which is reported to direct the elastase selectivity of these inhibitors (12). Thus, the P3 site of ShPI-1/K13L represents a potential candidate for modifying its activity against HNE or PPE. Supporting a previous report of a BPTI variant, our structural results will significantly contribute to selectivity modifications of BPTI-Kunitz-type inhibitors toward these enzymes in the future.

Experimental Procedures

Cloning and Production of ShPI-1/K13L—The gene of ShPI-1A was amplified by PCR with site-specific primers using the plasmid *pBM301* as a template; it was obtained previously for *rShPI-1A* expression (37). The purified product was cloned into the XhoI/XbaI-digested pPICZαA vector (Invitrogen). The mutation K13L was introduced according to the QuikChange® II XL protocol (Stratagene) using the mutagenic primers 5′-TCGGCCGTTGCCTAGGTTACTTCCC-3′ (sense) and 5′-GGGAAGTAACCTAGGCAACGGCCGA-3′ (antisense). These primers carried the desired mutations (underlined) and an XmaJI (AvrII) restriction site (C ↓ CTAG) for detection of positive clones. The variant protein was produced, purified, and stored following the previously established protocol for recombinant wild-type *rShPI-1A* (37). Protein production and purification was followed by SDS-PAGE (39). Inhibitory activity was determined by measuring the residual activity of pancreatic chymotrypsin (EC 3.4.21.1) at 25 °C with Suc-Ala-Ala-Pro-Phe-pNA as a substrate (40). The identity of *rShPI-1/K13L* was verified by molecular mass determination applying MALDI-TOF MS (Biflex spectrometer, Bruker Daltonics) using α-cyano-4-hydroxycinnamic acid as a matrix.

Specificity Studies and Determination of the Equilibrium Dissociation Constants (K_i)—The enzyme specificity of the *rShPI-1/K13L* inhibitor was determined using the serine proteases trypsin (EC 3.4.21.4, Sigma), HNE (EC 3.4.21.37), PPE (EC 3.4.21.36), and *Bacillus licheniformis* subtilisin A (EC 3.4.21.62), all from Calbiochem-Novabiochem. After incubation with *rShPI-1/K13L* for 10–30 min at 25 °C, residual enzymatic activities were measured by monitoring the cleavage of the specific substrates Bz-Arg-pN (for trypsin (41)) and MeO-Suc-Ala-Ala-Pro-Val-pNA (for HNE (42)), both of which are from Calbiochem-Novabiochem, as well as Suc-Ala-Ala-Ala-pNA from Sigma (for PPE (42)) and Suc-Ala-Ala-Pro-Phe-pNA from Bachem (for subtilisin A (43)).

The active concentration of *rShPI-1/K13L* was determined using a constant active concentration of chymotrypsin, previously titrated with soybean trypsin inhibitor. The latter was titrated with a known active concentration of trypsin that was

Crystal Structure of ShPI-1/K13L in Complex with Elastase

determined previously (44). All experiments were performed under titration conditions ($E_o/K_i \geq 100$). The formation of equimolar enzyme-inhibitor complexes was consistently assumed. Apparent inhibition constants ($K_{i,app}$) were determined as described (45), by fitting the steady state velocities to the equation for tight-binding inhibitors (46). Nonlinear regression analysis was performed using GraFit v.3.01 (47). Real K_i values were calculated using the equation $K_i = K_{i,app}/([S_o]/(K_m) + 1)$, considering the substrate concentration $[S_o]$ and their reported K_m values (40–42). Inhibitory activities were additionally determined at different incubation times and substrate concentrations.

Complex Formation and Crystallization—The binary complex rShPI-1/K13L·PPE was formed by incubating PPE with a 2-fold molar inhibitor excess in 15 mM phosphate buffer, pH 7.0, and 50 mM NaCl for 1 h at 25 °C. Complex formation was assessed by detecting the intensity fading of the inhibitor signal on a MALDI mass spectrum upon the addition of the enzyme immobilized on glioxal Sepharose® 4B as described for similar complexes (48). The complex was purified using HiLoad 16/60 Superdex-75 size exclusion chromatography column (GE Healthcare) equilibrated in the same buffer and concentrated to 18.0 mg/ml (Centricon 10-kDa molecular weight cut-off concentration devices, Millipore). The protein concentration was determined by absorbance at 280 nm using a theoretical extinction coefficient ($E_{280\text{ nm}}^{1\%}$) of 1.80 calculated for the complex with ProtParam (49) based on both protein sequences. Sample monodispersity and the hydrodynamic radius of the protein complex were evaluated by dynamic light scattering techniques as described previously (35, 38).

The screening of crystallization conditions was performed at 14 °C using the sitting drop vapor diffusion method in 96-well NeXtal plates (Qiagen). Protein solutions (300 nl) were mixed 1:1 (v/v) with commercially available reservoir solutions using a Honeybee 961 robot (Genomic Solutions). A monoclinic crystal (space group C2) of the rShPI-1/K13L·PPE complex measuring up to $550 \times 90 \mu\text{m}$ was detected when checking the plates after 1 year in condition 57 of the Qiagen Cryo Suite, which contained 0.425 M $(\text{NH}_4)_2\text{SO}_4$, 0.85 M Li_2SO_4 , 85 mM tri-sodium citrate, pH 5.6, and 15% glycerol.

Data Collection, Structure Determination, and Refinement—X-ray diffraction data were collected at the consortium's beamline X13 at HASYLAB (DESY, Hamburg, Germany) equipped with a MARresearch CCD detector. A single crystal was mounted in a nylon loop and flash-cooled in a nitrogen gas stream at 100 K. Diffraction images were processed and scaled using MOSFLM and SCALA (50). The structure was solved by molecular replacement using PHASER (51). The coordinates of free rShPI-1A (PDB code 3OFW (38)) and of free pancreatic elastase (PDB code 1QNJ (52)) were used as search models. Structure refinement was performed by alternate cycles of manual model rebuilding using COOT (53) and automated refinement (including isotropic B-factor refinement) applying Phenix software suite (54). As a test set for cross-validation, 5% of the reflections were randomly selected. In the final model, 207 water molecules as well as eight sulfate ions and seven glycerol molecules were added. Data collection and refinement statistics are provided in Table 1.

TABLE 1

Data collection and refinement statistics for rShPI-1/K13L·PPE

Values in parentheses refer to the highest resolution shell. $R_{p.i.m}$ represents the precision-indicating merging R factor as defined below.

Data collection	
Protein Data Bank code	3UOU
Space group	C2
Cell dimensions	
<i>a</i> , <i>b</i> , <i>c</i> (Å)	132.65, 47.18, 42.68
β (°)	100.07
Wavelength (Å)	
Resolution ^a (Å)	29.6–2.0 (2.10–2.00)
R_{merge}^a (%)	8.0 (25.7)
$R_{p.i.m.}^b$ (%)	3.7 (13.4)
R_{meas}^c (%)	7.7 (26.7)
No. of total reflections	70,731
No. of unique reflections	17,481
Mean I/σ	13.6 (6.2)
Completeness (%)	96.8 (99.9)
Multiplicity	4.0 (3.6)
Refinement	
Resolution (Å)	29.6–2.0 (2.10–2.00)
No. of reflections	17,120
$R_{\text{work}}/R_{\text{free}}$ (%)	16.6/21.1
No of protein/water/other atoms	2,242/206/82
No. of reflections used in R_{free}	892
Average B-factor (Å ²)	
Main-chain/side-chain atoms	25.4/28.4
Ligand (glycerol)/ion (sulfate)	48.4/41.5
Water	27.9
Root mean square deviations	
Bond length (Å)	0.01
Bond angles (°)	1.05
Residues in Ramachandran plot (%)	
Most favored	94.9
Allowed	5.1

$$^a R_{\text{merge}} = \frac{\sum_{hkl} \sum_i |I_i(hkl) - \langle I(hkl) \rangle|}{\sum_{hkl} \sum_i I_i(hkl)}$$

$$^b R_{p.i.m.} = \frac{\sum_{hkl} \{1/[N(hkl) - 1]\}^{1/2} \times \sum_i |I_i(hkl) - \langle I(hkl) \rangle|}{\sum_{hkl} \sum_i I_i(hkl)}$$

$$^c R_{\text{meas}} = \frac{\sum_{hkl} \{N(hkl)/[N(hkl) - 1]\}^{1/2} \times \sum_i |I_i(hkl) - \langle I(hkl) \rangle|}{\sum_{hkl} \sum_i I_i(hkl)}$$

Structure Analysis—The stereochemical quality of the model was evaluated using VERIFY-3D (55), and MOLPROBITY (56). Interface calculations were performed using the PISA server (57). Analyses of atom-atom contacts and structural superposition were done using the WHAT IF program (58). The CryCo server was used for analysis of crystal contacts (59). PPE residues at the interface were numbered according to their similar topology with chymotrypsinogen (UniProt accession number P00766). Figs. 1, *a* and *b*, and 2–6 were generated with PyMOL (60).

Results

Cloning, Production, and Purification of rShPI-1/K13L—The variant protein rShPI-1/K13L was produced in *Pichia pastoris*, yielding a level of 60 mg inhibitor/liter culture broth. A single cation exchange chromatography resulted in a pure inhibitor fraction, as confirmed by a single protein band on SDS-PAGE and a single peak in MALDI-TOF MS analysis. The molecular weight of 6096.47 Da ($M+H^+$, 6097.47 Da) detected for the intact protein agrees with the expected value for the variant rShPI-1/K13L (6096.82 Da). In contrast to previous results with BPTI (61, 62), the correct processing of the α -factor-ShPI-1 fusion without the N-terminal motif Glu-Ala-Glu-Ala was obtained here. Peptide mass mapping after tryptic digestion verified the entire protein sequence including the K13L exchange. The experimental masses of three peptides (Cys¹²-Arg¹⁸, 912.46 Da; Lys⁸-Arg¹⁸, 1352.75 Da; and Val⁹-Lys²⁷, 2243.23 Da) agreed with the calculated values, considering the presence of Leu at the mutated P1 position of the inhibitor.

TABLE 2**Real inhibition constants (K_i) of rShPI-1A wild type and K13L variant for serine proteases**

K_i values are reported in nM. NI, no inhibition was detected even at I_0/E_0 molar ratio of 170 incubated for 30 min. Real K_i values were calculated according to the equation $K_i = K_{i,app}/([S_0]/(K_m) + 1)$ considering the substrate concentration $[S_0]$ and the K_m values. The following substrates were used for: trypsin, Bz-Arg-pNA (41); HNE, MeO-Suc-Ala-Ala-Pro-Val-pNA (42); chymotrypsin, Suc-Ala-Ala-Pro-Phe-pNA (40); and PPE, Suc-Ala-Ala-Ala-pNA (42).

Enzyme	rShPI-1A wt	rShPI-1/K13L
Trypsin	2.7 ± 0.3	320 ± 35
Chymotrypsin	14.8 ± 1.5	4.5 ± 0.5
Human neutrophilic elastase	23.5 ± 2.0	1.3 ± 0.4
Porcine pancreatic elastase	NI	12.0 ± 2.6

Inhibitory Activity of rShPI-1/K13L—Incubation of trypsin, chymotrypsin, and HNE with rShPI-1/K13L resulted in an inhibition of these serine proteases consistently characterized by K_i values within the nanomolar range (Table 2) as described previously for the natural and recombinant wild type-like inhibitors (21, 37). Solely the binding affinity to trypsin is significantly decreased (~100-fold) as a result of the mutation, whereas rShPI-1/K13L appears to be slightly more potent against chymotrypsin and HNE than the wild-type inhibitor. In agreement with previous mutagenesis studies of BPTI (25–28), the replacement of the large basic Lys residue against the smaller hydrophobic leucine residue transformed rShPI-1/K13L into a high-affinity PPE inhibitor. This additional activity has never been observed for natural or wild-type rShPI-1A, even if an I_0/E_0 molar ratio of 170 is used (21, 37). The PPE inhibition activity was stable after incubation for 15 s, indicating that the enzyme, the inhibitor, and the substrate as well as their complexes were in equilibrium. The observed substrate dependence of the PPE inhibition (residual enzyme activity increased with substrate concentration) is characteristic for a competitive mechanism. Moreover, the concave inhibition curves recorded under the experimental conditions of $[E_0]/K_i = 1–10$ (data not shown) showed that rShPI-1/K13L is a reversible and tight-binding inhibitor of all four enzymes.

Crystallization and Structure Determination of rShPI-1/K13L in Complex with PPE—Prior to crystallization trials, specific complex formation between rShPI-1/K13L and PPE was confirmed by intensity-fading MALDI-TOF MS, dynamic light-scattering measurements, and size exclusion chromatography (data not shown). The purified rShPI-1/K13L-PPE complex formed monoclinic crystals belonging to the space group C2 and diffracted up to a resolution of 2.0 Å. The asymmetric unit contained one complex molecule. After structure determination by molecular replacement using the coordinates of free PPE (PDB code 1QNJ) and free wild-type rShPI-1A (PDB code 3OFW) as search models, the entire PPE polypeptide as well as all inhibitor residues at the complex interface could be traced completely in the electron density map. Only the β -hairpin segment Phe²¹-Lys²⁷ of the inhibitor and its C-terminal residue Ala⁵⁵ are poorly defined because of increased flexibility. All residues are located within the most favored or allowed regions of the Ramachandran plot, reflecting the quality of the rShPI-1/K13L-PPE structure. The details of data collection and refinement statistics are presented in Table 1.

Overall Structure—The overall fold of the rShPI-1/K13L-PPE complex closely resembles that expected for an interaction of a

serine protease and a canonical inhibitor (Fig. 1a) (32–35). The complex interface buries an inhibitor surface area of 865.7 Å² (23.7% of its total solvent-accessible surface), which is slightly increased compared with rShPI-1A complexes with trypsin (765.1 Å² and 18.2%) and chymotrypsin (787.4 Å² and 21.2%). This is due to an extended interface involving residues Lys⁸ (P6) to Arg¹⁸ (P5') located at the primary binding loop of rShPI-1/K13L, as well as a secondary interaction site comprising the inhibitor residues Ile³² to Gly³⁸. Both interaction loops are stabilized by the disulfide bond Cys¹²-Cys³⁶, keeping the primary loop in a well ordered conformation, which enables the formation of an antiparallel β -sheet within the concave binding pocket of PPE (Fig. 1b) that is typical for canonical inhibitors. An enzyme surface area of 706.5 Å² (6.7%) is buried in the complex, which is slightly lower than that in the PPE complexes with the canonical inhibitors HEI-TOE (7.3%), elafin (7.6%), and C/E-1 (8.6%).

Neither the K13L variant nor the PPE interaction significantly affected the overall inhibitor fold, as indicated by a root mean square deviation of 0.532 Å over 54 superposed C α atoms of unbound wild-type rShPI-1A (PDB code 3OFW) and PPE-bound rShPI-1/K13L. Deviations of up to 1.2 Å observed at Arg¹¹ (P3), Tyr¹⁵ (P2'), and His⁴⁷ to Gln⁴⁸ are most likely attributable to the high B-factors and crystal contacts identified previously at these positions in the crystal structure of free rShPI-1A (PDB code 3OFW). Additional deviations have been detected for Ser²³ to Thr²⁵, but these β -hairpin residues are largely undefined within the electron density map as mentioned previously. Likewise, native and inhibitor-bound PPE (PDB code 3EST) showed no significant structural differences (root mean square deviation of 0.568 Å over 240 superposed C α atoms). The positions of the catalytic residues His⁵⁷, Asp¹⁰² and Ser¹⁹⁵, as well as Ser¹⁸⁹ and Gly¹⁹³ within the S1 pocket, remained highly conserved in both enzyme molecules. In contrast, enzyme residues at other prime and non-prime subsites were slightly affected by inhibitor binding. Significant deviations of up to 2.3 Å (C α positions) were detected in the loop region Arg¹⁴⁵-Gln¹⁵⁰ close to the S2' site (Leu¹⁴³/Leu¹⁵¹), at Ser^{36C}/Ser³⁷ and Asp⁶⁰/Arg⁶¹ near the Sn' sites, as well as at the calcium-binding loop of the elastase (Asn⁷⁴-Gly⁷⁸). However, according to CryCo server analysis, most of these displacements may also be attributed to the differences detected in the crystal packing environments.

rShPI-1/K13L-PPE Interface and Comparison with the rShPI-1A-trypsin Complex—In common with other canonical inhibitors, the primary direct interactions of rShPI-1/K13L with PPE are provided by residues at positions P2, P1, and P1' of the primary binding loop, which are completely buried due to complex formation (Fig. 1c). Compared with the interface of trypsin-bound rShPI-1A (PDB code 3M7Q) (35), residues Gly¹⁰ (P4), Tyr¹⁵ (P2'), and Pro¹⁶ (P3') provide an increased contribution to the elastase interaction, whereas the impact of Arg¹¹ (P3) and Pro¹⁷ (P4') is slightly reduced. The rShPI-1/K13L-PPE interface is extended by one residue at both sites of the scissile bond compared with known complexes of BPTI and rShPI-1A with trypsin (32–35). The accessible surface area of the outer residues, Lys⁸ (P6) and Arg¹⁸ (P5'), is buried by more than 30% after complex formation with PPE (Fig. 1c), whereas these res-

Crystal Structure of ShPI-1/K13L in Complex with Elastase

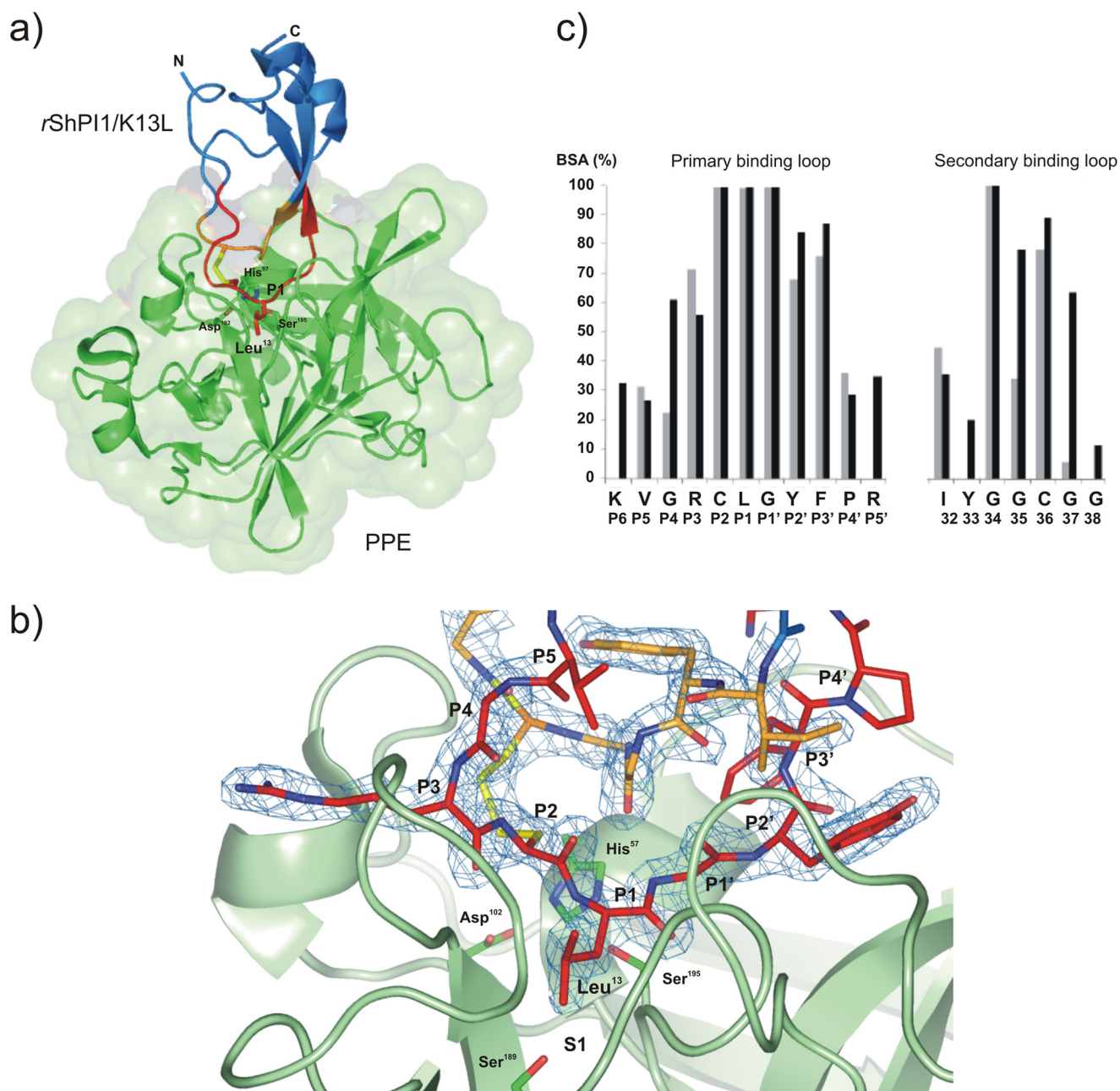


FIGURE 1. Structure of the rShPI-1/K13L-PPE complex (PDB code 3UOU). *a*, schematic model of the overall structure of the complex between PPE (green, surface representation) and rShPI-1/K13L (blue), showing the changed P1 residue Leu¹³ of the inhibitor in stick representation. The primary (P6-P5' sites) and secondary binding loops are highlighted in red and orange, respectively, and the linking disulfide bridge, Cys¹²-Cys³⁶, is shown in yellow. *b*, close view of the entire complex interface centered on the S1 pocket of PPE, illustrating the formation of an antiparallel β -sheet by the inhibitor loops within the concave binding pocket of the enzyme that is typical for canonical inhibitors. The binding loops of rShPI-1/K13L (stick representation) are well defined by the $2F_o - F_c$ map (blue) countered at 1σ . The side chains of the catalytic triad residues His⁵⁷, Asp¹⁰², and Ser¹⁹⁵ as well as Ser¹⁸⁹ at the bottom of the S1 pocket of PPE are highlighted in stick representation. *c*, buried surface area (BSA) of rShPI-1/K13L residues (black) involved in the PPE interface compared with that of wild-type rShPI-1A (gray) bound to trypsin. The buried surface area represents a percentage of the total surface area that is buried after complex formation. The amino acid sequence of rShPI-1/K13L and the corresponding Pn sites are shown.

idues do not show any contribution to the rShPI-1A-trypsin complex (35). An overall number of 156 direct enzyme-inhibitor contacts is shorter than 4 Å, including 144 hydrophobic contacts and 10 hydrogen bonds; these are involved in the stabilization of the rShPI-1/K13L-PPE interface (Table 3). This is a slight increase compared with the trypsin complex (116 hydrophobic contacts and 10 H-bonds) (35). Direct H-bonds are provided by Arg¹¹ (P3), Leu¹³ (P1), Gly¹⁴ (P1'), and Tyr¹⁵ (P2') at the canonical loop segment, as well as by Gly³⁵ and Gly³⁷ at the

secondary binding loop. Further interface stabilization is provided by polar interactions mediated by 10 water molecules connecting the P4, P3, and P2' sites as well as Ile³², Gly³⁵, and Gly³⁷ of rShPI-1/K13L with corresponding subsites in PPE (Table 4).

At the modified P1 position of rShPI-1/K13L, Leu¹³ accounts for 27% of the direct interactions with PPE. All backbone atoms share equivalent positions compared with the rShPI-1A-trypsin complex (35) (Fig. 2). In agreement with the general serine pro-

TABLE 3

Enzyme-inhibitor interactions in the PPE complex of rShPI-1/K13L

PPE residues are numbered according to their similar topology with chymotrypsinogen. The total number of contacts between a pair of residues (≤ 4.0 Å) is shown in parentheses, then the closest atoms are listed, and distances (Å) are given in square brackets. Hydrogen bonds, displayed in a bold underlined font, were scored using the PDBe PISA server (57), applying the following parameters: maximal donor-acceptor distance, 3.50 Å; maximal hydrogen-acceptor distance, 2.50 Å; maximal angular errors, 90.00. Enzyme residues Arg^{217A} and Ala^{99A} represent native insertions in the sequence of PPE as compared with chymotrypsin.

rShPI-1/K13L residue	PPE residue	(Total contacts) Closest atoms [distance]
P6 Lys ⁸	Arg ^{217A}	(6) CE--NH2 [3.59]
P5 Val ⁹	Gln ¹⁹²	(1) CG1--NE2 [3.83]
P4 Gly ¹⁰	Arg ^{217A}	(2) C--CG [3.82]
P3 Arg ¹¹	Ala ^{99A}	(1) NH1--CB [3.87]
	Thr ¹⁷⁵	(1) NH2--OG1 [3.90]
	Phe ²¹⁵	(5) O--CB [3.10]
	Val ²¹⁶	(10) O--N [2.82]
	Arg ^{217A}	(3) CG--CG [3.47]
P2 Cys ¹²	His ⁵⁷	(8) CB--NE2 [3.52]
	Val ⁹⁹	(2) SG--CG2 [3.76]
	Gln ¹⁹²	(4) O--OE1 [2.97]
	Ser ²¹⁴	(3) CA--O [3.51]
P1 Leu ¹³	His ⁵⁷	(1) N--NE2 [3.86]
	Gly ¹⁹⁰	(3) CD1--C [3.47]
	Cys ¹⁹¹	(6) CD2--C [3.56]
	Gln ¹⁹²	(9) CA--OE1 [3.37]
	Gly ¹⁹³	(4) O--N [2.73]
	Asp ¹⁹⁴	(1) O--N [3.26]
	Ser ¹⁹⁵	(11) C-OG [2.76]; O--N [3.04]
	Thr ²¹³	(1) CD1--CG2 [3.78]
	Ser ²¹⁴	(1) N--O [3.33]
	Val ²¹⁶	(4) CD2--CG2 [3.52]
P1' Gly ¹⁴	Thr ⁴¹	(2) C--O [3.86]
	His ⁵⁷	(1) N--NE2 [3.75]
	Gln ¹⁹²	(5) O--OE1 [3.02]
	Gly ¹⁹³	(2) C--N [3.58]
	Ser ¹⁹⁵	(4) N--OG [3.02]
P2' Tyr ¹⁵	His ⁴⁰	(1) CD2--O [3.87]
	Thr ⁴¹	(8) N--O [3.00]
		N--OG1 [3.80]
	Leu ¹⁴³	(2) CE1--CD1 [3.71]
	Leu ¹⁵¹	(11) CD1--CD2 [3.47]
	Gly ¹⁹³	(3) CB--CA [3.69]
P3' Phe ¹⁶	Thr ⁴¹	(5) CZ--OG1 [3.62]
	Cys ⁵⁸	(1) CZ--O [3.63]
	Arg ⁶¹	(4) CZ--NE [3.54]
	Tyr ³⁵	(2) CE1--OE1 [3.26]
P4' Pro ¹⁷	Arg ⁶¹	(1) NH2--NH1 [3.22]
P5' Arg ¹⁸	Gln ¹⁹²	(1) CG2--CB [4.00]
32 Ile ³²	His ⁵⁷	(2) O--CD2 [3.64]
34 Gly ³⁴	Gln ¹⁹²	(1) CA--OE1 [3.70]
	His ⁵⁷	(2) O--O [3.56]
35 Gly ³⁵	Arg ⁶¹	(3) O--NH2 [2.77]
	Thr ⁹⁶	(4) CB--O [3.58]
36 Cys ³⁶	Val ⁹⁹	(2) SG--CB [3.84]
	Thr ⁹⁶	(2) N--O [2.91]
37 Gly ³⁷		

tease catalysis and substrate-like inhibition mechanisms, the carbonyl oxygen atom of Leu¹³ occupies the oxyanion hole, establishing three hydrogen bonds to the backbone nitrogen atoms of PPE residues Gly¹⁹³, Asp¹⁹⁴, and Ser¹⁹⁵, together with an H-bond to Ser²¹⁴ via its nitrogen atom. The hydrophobic side chain of Leu¹³ sticks into the hydrophobic S1 pocket of PPE formed by the enzyme residues Gly¹⁹⁰, Thr²¹³, and Val²¹⁶, as well as the hydrophobic parts of the Gln¹⁹² and Cys¹⁹¹ side chains, establishing important van der Waals contacts that stabilize the interaction. As expected, Leu¹³ at P1 is not involved in water-mediated interactions, in contrast to Lys¹³ in the trypsin complex of the wild-type inhibitor (35). Moreover, the shorter side chain of Leu¹³ at the mutated P1 site cannot interact with PPE residues 189, 190, 215, and 216, as observed in the trypsin complex of the wild-type inhibitor (Fig. 2).

TABLE 4

Water-mediated hydrogen bonds at the interface of the rShPI-1/K13L-PPE complex

PPE residues are numbered according to their similar topology with chymotrypsinogen. Numbers in parentheses refer to donor-acceptor distances (Å). Water molecules (W) are labeled according to the numbers in the PDB file, in which they are assigned to the enzyme (e) or inhibitor (i) chains. The suffix "A" indicates amino acid insertions in the PPE sequence compared to that of chymotrypsinogen. The following parameters were used to identify an H-bond: maximal donor-acceptor distance, 3.50 Å; maximal hydrogen-acceptor distance, 2.50 Å; maximal angular errors, 90.00.

Position	K13L-PPE
	Å
P4	Gly ¹⁰ⁱ O--W ⁶⁵ⁱ (3.05)
	W ⁶⁵ⁱ -Arg ^{217Ae} (3.22)
	Gly ¹⁰ⁱ O--W ^{304e} (2.84)
	W ^{304e} --Gln ^{192e} OE1 (2.84)
P3	Arg ¹¹ⁱ NH1--W ⁷²ⁱ (2.86)
	W ⁷²ⁱ --Asp ^{97e} OD1 (3.03)
	W ⁷²ⁱ --Ala ^{99Ae} N (3.06)
	W ⁷²ⁱ --W ⁵⁹ⁱ (3.68)--Val ^{99e} N (3.05)
P2'	Tyr ¹⁵ⁱ OH--W ⁶⁶ⁱ (2.69)
	W ⁶⁶ⁱ --Gln ^{150e} OE1 (2.99)
	W ⁶⁶ⁱ --Gly ^{149e} O (2.77)
	Tyr ¹⁵ⁱ OH--W ^{358e} (3.28)
	W ^{358e} --Leu ^{151e} N (2.89)
2nd loop	Ile ³²ⁱ O--W ⁶⁰ⁱ (2.88)--W ^{315e} (3.67)
	W ^{315e} --Gln ^{192e} NH1 (2.87)
	Gly ³⁵ⁱ O--W ^{293e} (2.74)
	W ^{293e} --Thr ^{96e} OG1 (2.60)
	Gly ³⁷ⁱ N--W ^{295e} (3.43)
	W ^{295e} --Thr ^{96e} OG1 (2.61)

The canonical segment of the primary inhibitor binding loop (positions P3--P3') of rShPI-1/K13L adopts a well conserved conformation that is comparable within the PPE and the trypsin complexes of ShPI-1. Direct superposition reveals only slight rearrangements of side-chain atoms at the P3 site (Arg¹¹) because of its specific adaptation to the S3 pocket of PPE (Fig. 3a). As a consequence, two additional H-bonds detected previously in the rShPI-1A-trypsin complex (35) are absent, and only the typical H-bond with the nitrogen atom of residue 216 remains conserved. Additional differences at the non-prime side are detected at position P4, where Gly¹⁰ interacts with the inserted Arg^{217A} of PPE that is absent in trypsin (35). At the prime subsite of the primary binding loop, residue Tyr¹⁵ (P2') of rShPI-1/K13L is involved in several direct and water-mediated H-bonds with PPE (Fig. 3b), whereas only one H-bond stabilizes the trypsin complex at the P2' position (35). In contrast, the hydrophobic contacts established between Pro¹⁷ (P4') and the enzyme residue Tyr³⁹ in the ShPI-1-trypsin complex are reduced here (Table 3), as the bulky hydrophobic site chain of Tyr³⁹ is replaced by Ala in PPE. Moreover, additional van der Waals contacts of the hydrophobic part of the Lys⁸ side chain (P6) with the carbon moiety of Arg^{217A} in PPE as well as side-chain interactions between Arg¹⁸ (P5') and Arg⁶¹ in PPE (3.2 Å) extend the interface compared with the trypsin complex, as mentioned previously.

Residues located at the secondary binding loop of rShPI-1/K13L (Ile³² to Gly³⁸) are significantly more involved in the interaction with PPE than with trypsin. The buried surface area of all corresponding rShPI-1/K13L residues is obviously increased compared with equivalent residues within the trypsin complex (Fig. 1c). Gly³⁵ and Gly³⁷ establish direct H-bonds with Arg⁶¹ and Thr⁹⁶ of PPE, in addition to water-mediated interactions (Fig. 4). The entire secondary loop accounts for

Crystal Structure of ShPI-1/K13L in Complex with Elastase

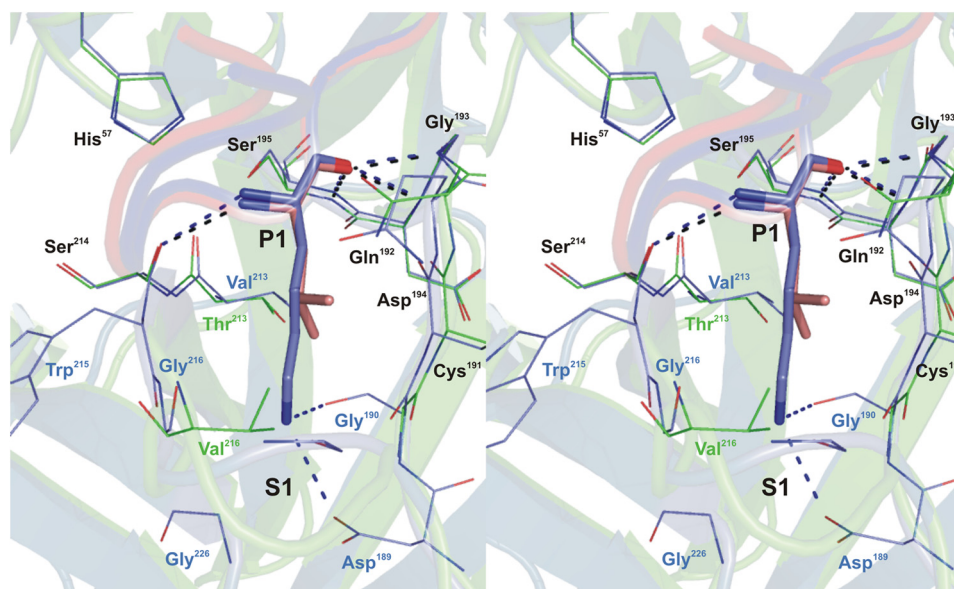


FIGURE 2. Stereo view of the P1-S1 interaction at the *rShPI-1/K13L*-PPE complex interface compared with that in the trypsin complex of wild-type *rShPI-1A* (35). Enzyme residues involved in inhibitor contacts are shown as a line representation (PPE, green; trypsin, blue), and primary binding loop residues of *rShPI-1/K13L* (salmon) and wild-type *rShPI-1A* (blue) are displayed as sticks. Conserved residues are labeled in black, and non-conserved residues are in the same color as the corresponding enzyme. Hydrogen bonds are represented by black (PPE) and blue (trypsin) dashed lines. To simplify the figure, water molecules that are present in the trypsin complex (35) around the P1 position are not included. For details of the interactions in the *rShPI-1/K13L*-PPE complex, see Tables 3 and 4.

hydrophobic contacts with PPE residues His⁵⁷, Arg⁶¹, Thr⁹⁶, Val⁹⁹, and Gln¹⁹² (Table 3). In contrast, no H-bonds and significantly less van der Waals contacts are provided by the secondary binding loop upon trypsin binding (35). Glu⁴⁴, located C-terminally outside of this loop in *rShPI-1/K13L*, is also slightly buried after complex formation, establishing an interaction with Arg⁶¹ of PPE (OE2-NH1) characterized by a longer than usual distance for a salt bridge (~ 5.0 Å). All of these interactions are favored in PPE because of the increased length of the loop structures containing residues 61–64 and 97–99 as compared with trypsin (Fig. 4).

Comparison with Elastase Complexes of Other Canonical Inhibitors—As expected, all of the main contacts to PPE established by the P1 site of *rShPI-1A/K13L* are highly conserved compared with the canonical inhibitors elafin (P1, Ala), C/E-1 (P1, Leu), and HEI-TOE (P1, Leu) belonging to the WAP, *Ascaris*, and Kazal/squash families, respectively (14–16). Main differences are thus restricted to the prime/non-prime subsites of the interface. An unusually large buried surface area is reported for PPE in complex with the *Ascaris* inhibitor C/E-1 (8.6%), mainly because of the deep penetration of Ser²¹⁷ into an inhibitor surface pocket formed by positions P15 to P13 and P10' to P13' (15). This has not been detected in other elastase/canonical inhibitor complexes. Similar to the *rShPI-1/K13L*-PPE complex presented here, a shorter primary interaction segment comprising the P5 to P2' sites together with a three-residue secondary binding loop is reported for elafin (14). The hybrid squash inhibitor binds via well defined interactions at positions P4 to P4', supported by five additional weak contacts to the elastase (16). Concordantly, the inhibition strength of C/E-1 is the highest ($K_i = 0.063$ nmol/liter (63), whereas similar K_i values have been reported for the inhibitors elafin (6.0 nmol/liter (14) or 1.0 nmol/liter (64)) and HEI-TOE (0.98 nmol/liter

(16)), almost comparable with *rShPI-1/K13L* (12 nmol/liter) reported in this study.

To obtain first insights into the structural determinants for an interaction with HNE, we compared the *rShPI-1/K13L*-PPE interface with that of the chelonians elafin (P1, Ala²⁴) and 1/2SLPI (P1, Leu⁷²) in complex with PPE and HNE, respectively. Chelonians represent the only family of canonical inhibitors with three-dimensional structures determined for complexes with both elastases (12, 14). As expected for canonical inhibitors from different families, the backbone conformation of the canonical P3–P3' segment is similar among these inhibitors, but differences have been detected for flanking residues (19, 65). Most noteworthy, the side chain of Arg¹¹ at the P3 site of the Kunitz-type inhibitor *rShPI-1/K13L* extends into a similar enzyme region as the residues at the P5 position of the chelonians elafin and 1/2SLPI (Fig. 5). Thus, Arg¹¹ of *rShPI-1/K13L* interacts with residue Thr¹⁷⁵ within the PPE surface loop segment Ser¹⁶⁹–Val¹⁷⁶, which is defined as the S5 pocket in the elafin-PPE complex (12, 14). In addition, the P3 site of *rShPI-1/K13L* (Arg¹¹) interacts with Ala^{99A}, Phe²¹⁵, Val²¹⁶, and Arg^{217A} of PPE (Table 3) and is indirectly H-bonded to Asp⁹⁷, Val⁹⁹, and Ala^{99A}. These residues represent insertions into the sequence of PPE that cause remarkable structural differences in the loops in which they are located, as compared with similar regions of HNE (Fig. 5). Accordingly, the P3 site of ShPI-1 may contribute to differences in selectivity toward HNE and PPE.

Discussion

The interaction between BPTI-Kunitz-type inhibitors and serine proteases from the chymotrypsin family has been well studied. However, the known three-dimensional structures of enzyme complexes with inhibitors of this family are limited to trypsin- and chymotrypsin-like enzymes (32–35). The inhibitor specificity is

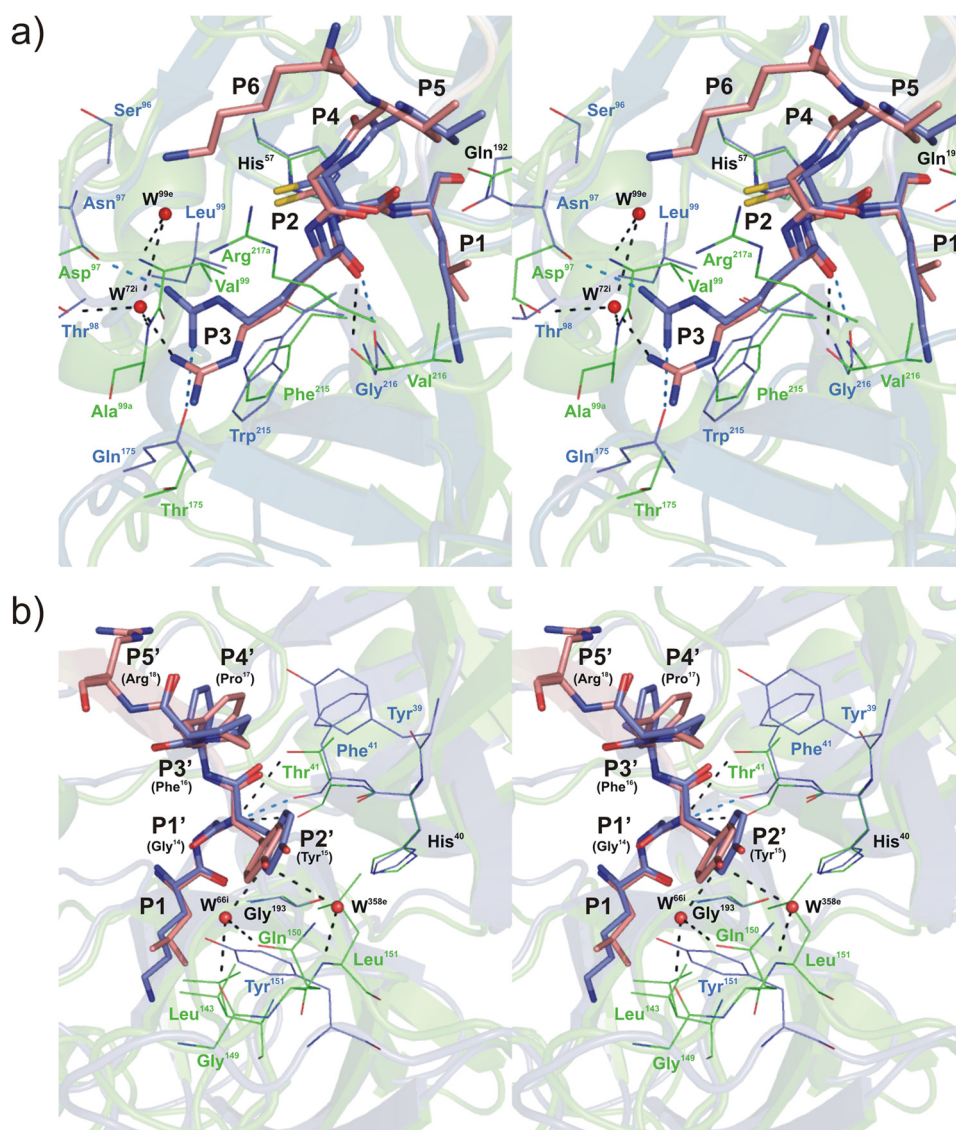


FIGURE 3. Stereo view of the *rShPI-1/K13L*-PPE complex interface superposed with that of wild-type *rShPI-1A* in complex with trypsin (35) at the *Pn* (a) and *Pn'* (b) site of the primary inhibitor binding loop. Enzyme residues involved in inhibitor contacts are shown in line representation (PPE, green; trypsin, blue; conserved residues His⁵⁷ and Gln¹⁹², black labels), and primary binding loop residues of *rShPI-1/K13L* (salmon) and wild-type *rShPI-1A* (blue) are displayed as sticks. The side chain at the P1 position of the inhibitor is included to enable a comparison with Figs. 1c and 2. Hydrogen bonds are represented by black (PPE) and blue (trypsin) dashed lines. Water molecules (W) are shown as red spheres and are labeled according to the PDB files in which they are assigned to the enzyme (e) or inhibitor (i) chains. Conformational differences between both complexes are restricted to position P3 at the Pn site of the primary binding loop. The P6 residue is only involved in the interface within the *rShPI-1/K13L*-PPE complex. For details of the interactions in the *rShPI-1/K13L*-PPE complex, see Tables 3 and 4.

usually categorized in terms of the P1-S1 interaction, mainly considering the enzyme residues at positions 189, 216, and 226 of the S1 pockets. In chymotrypsin, the combination of Ser¹⁸⁹, Gly²¹⁶, and Gly²²⁶ creates a deep hydrophobic pocket that correlates with the usual hydrophobicity of the P1 residue in a chymotrypsin substrate or inhibitor. In contrast, trypsin-like enzymes contain a negatively charged S1 site due to the presence of Asp¹⁸⁹ at the bottom, which accounts for their specificity against substrates containing Arg or Lys residues at P1 position.

The S1 pocket of elastase-like enzymes is significantly narrowed overall by more bulky side chains at positions 216 and 226, usually resulting in the recognition of small or medium-sized aliphatic P1 residues (11). At the bottom of the S1 pocket, the respective residue (Ser¹⁸⁹ in PPE or Gly¹⁸⁹ in HNE) is inaccessible to the P1 side chain of the inhibitor, as it is covered by

the hydrophobic parts of Ile¹³⁸ and Thr²²⁶ (in PPE) or Val¹⁹⁰ (in HNE). Compared with PPE, the S1 pocket of HNE shows an increased flexibility, enabling the adaptation to a broader variety of P1 side chains (11, 23). The largest backbone atom divergence between PPE and HNE at this side occurs at positions 192 (Gln¹⁹² in PPE and Phe¹⁹² of HNE) and 226 (Thr²²⁶ in PPE and Asp²²⁶ in HNE). Moreover, HNE harbors a negative charge from Asp²²⁶ (that replaces Thr²²⁶ of PPE) within its S1 pocket, which is largely shielded by Val²¹⁶ and Val¹⁹⁰. However, modeling studies with the Kazal-type inhibitor CmPI-2 suggest that penetration of a basic P1 side chain is still possible (24). A salt link with Asp²²⁶ is established, supported by additional contacts with Ser²¹⁴ and Ala²²⁷ of HNE, which were not detected for a homologous inhibitor that harbors Leu at P1 position. These unique characteristics of HNE could explain the selective

Crystal Structure of ShPI-1/K13L in Complex with Elastase

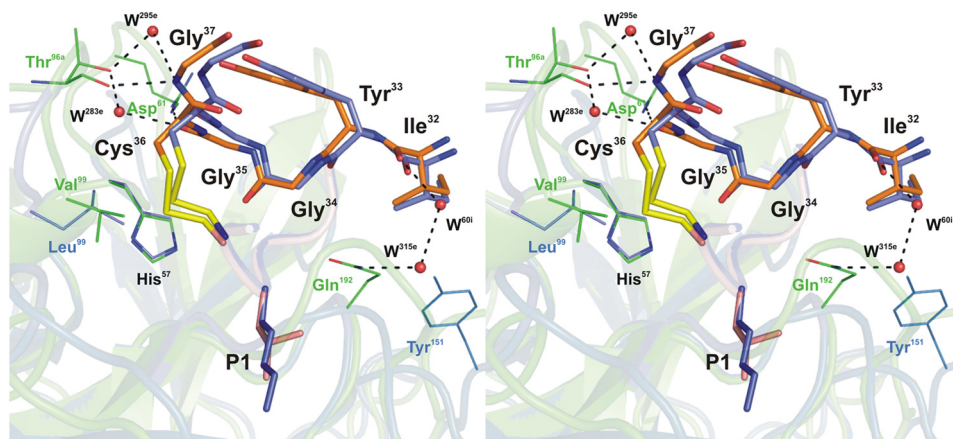


FIGURE 4. Stereo view of the *rShPI-1/K13L*-PPE complex interface maintained by the secondary binding loop superposed with that of wild-type *rShPI-1A* in complex with trypsin (35). Enzyme residues involved in inhibitor contacts are shown in *line* representation (PPE, green; trypsin, blue; conserved residue His⁵⁷, black). Secondary binding loop residues (Ile³²-Gly³⁷) of *rShPI-1/K13L* (orange) and wild-type *rShPI-1A* (light blue) are displayed as *sticks*, and the P3-P3' segment of the primary binding loop of both inhibitors is shown schematically (*rShPI-1/K13L*, salmon; *rShPI-1A*, dark blue) with *sticks* at the P1 side chain. Hydrogen bonds are represented by *black dashed lines*. Water molecules (*W*) are shown as *red spheres* and are labeled according to the PDB file in which they are assigned to the enzyme (*e*) chain. For details of the interactions, see Tables 3 and 4.

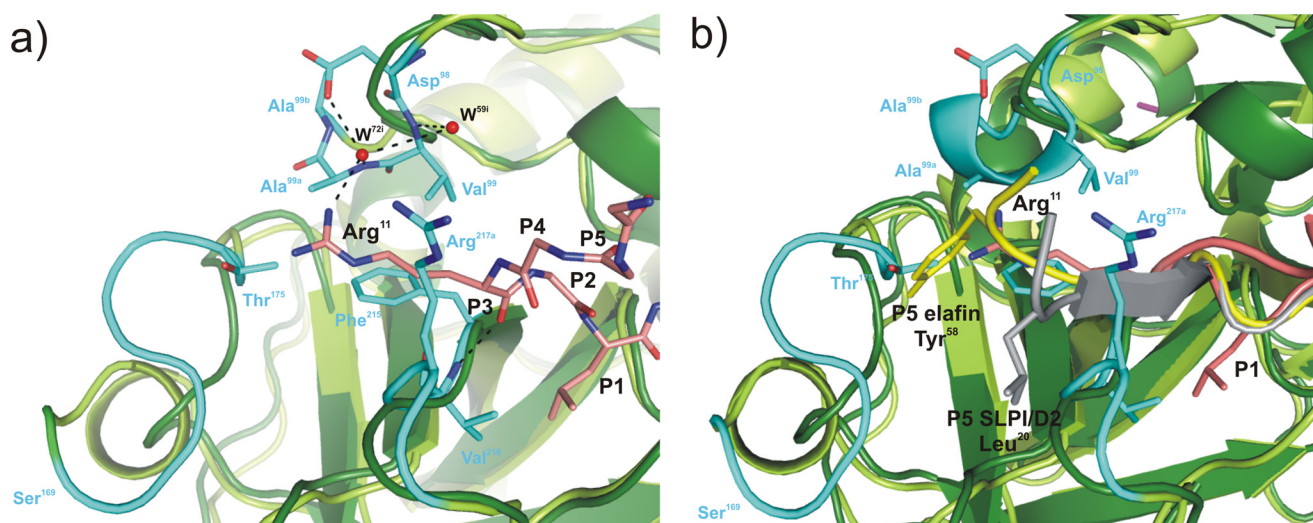


FIGURE 5. Structural superposition of elastases in complex with BPTI-Kunitz- and WAP-type inhibitors focused on the non-prime subsite of the primary binding loops of the inhibitors. *a*, interface between PPE (dark green, schematic representation) and *rShPI-1/K13L* (salmon, stick representation) around the P3 residue (Arg¹¹) at the P_n side of the primary binding loop (residues P6–P1). To highlight structural differences between elastases, the PPE structure is superposed with that of HNE (light green, PDB code 2Z7F), and PPE regions characterized by significant main chain deviations are highlighted in cyan. PPE residues interacting with the P3 residue of *rShPI-1/K13L* as well as the inhibitor side chains of Arg¹¹ (P3) and Leu¹³ (P1) are shown in *stick* representation. Hydrogen bonds are represented with *black dashed lines*. Water molecules (*W*) are shown as *red spheres* and are labeled according to the PDB file in which they are assigned to the inhibitor (*i*) chain. *b*, corresponding interface region in the PPE (dark green) and HNE (light green) complexes of the WAP inhibitors elafin (gray, PDB code 1FLE) and SLPI/D2 (yellow, PDB code 2Z7F), respectively, shown in schematically. The side chains of residues at their P5 sites, Tyr⁵⁸ in elafin and Leu²⁰ in SLPI/D2 (12), are highlighted as *sticks*.

elastase inhibitory activity determined for wild-type *rShPI-1A* and for BPTI (18), both of which contain Lys at position P1.

In PPE, the completely non-polar as well as rigid and narrow S1 site in turn prevents the efficient accommodation of the Lys side chain, as reported for the BPTI (32) and *rShPI-1A* complexes of chymotrypsin (PDB code 3T62)³ that comparably feature a deep hydrophobic S1 pocket. However, tight inhibitor binding to chymotrypsin is maintained by an alternative “up” conformation of the P1 Lys side chain instead of extending directly into the pocket (“down” conformation). This shift establishes a new set of H-bonds that compensate the interface stabilization, involving the NZ atom of Lys (inhibitor) and the

main-chain oxygen atom of Ser²¹⁷ at the entry of the chymotrypsin S1 site (32). The first crystal structure of a BPTI-Kunitz-type inhibitor in complex with an elastase-like enzyme reported in this study strongly indicates that a similar stabilization of the up conformation at the PPE S1 site is not possible. Although Ser²¹⁷ remains conserved within the PPE sequence, the insertion of Arg^{217A} promotes an altered conformation of the corresponding loop in PPE compared with other serine proteases, shifting Ser²¹⁷ around 4.7 Å away from the P1 side chain and thus preventing stabilizing interactions (Fig. 6). This is reflected by weak (BPTI (18)) or undetectable (*ShPI-1* (21)) binding of the wild-type inhibitors to PPE.

As observed previously for BPTI and in agreement with the preference for aliphatic residues at P1, a tight-binding inhibitor of

³ R. García-Fernández, R. Domínguez, D. Oberthuer, T. Pons, Y. González-González, M. A. Chávez, C. Betzel, and L. Redecke, unpublished observation.

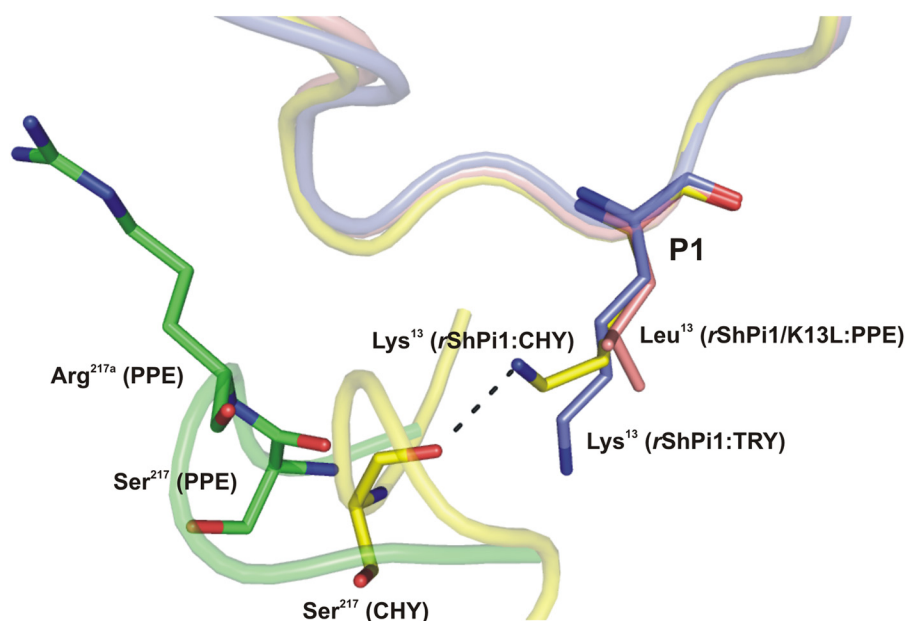


FIGURE 6. Superposition of the P1 side chain conformation of *rShPI-1/K13L* (salmon) in complex with PPE (green) compared with that of the wild-type inhibitor in complexes with trypsin (blue, PDB code 3MTQ) and chymotrypsin (yellow, PDB code 3T62). The inhibitor binding loops are shown schematically with the P1 residues in sticks. The insertion of Arg^{217A} in PPE triggers structural differences that prevent a stabilizing interaction of the basic P1 residue with Ser²¹⁷, as observed in the chymotrypsin complex (32). Here, the side chain of Lys¹³ adopts an up conformation, which is different from the down conformation in the trypsin complex (blue) and is stabilized by an H-bond with the oxygen atom of Ser²¹⁷. However, the insertion of Arg^{217A} in PPE (green) moves Ser²¹⁷ away from P1, suggesting that a similar stabilizing bond with basic residues at P1 is not possible.

both elastases, HNE and PPE, was obtained in this study by substitution of the P1 Lys residue of the BPTI-Kunitz-type domain ShPI-1 against Leu. The aliphatic side chain improves the hydrophobic interaction with the narrow S1 pocket, which is formed by Gly¹⁹⁰, Thr²¹³, and Val²¹⁶ in PPE. However, the overall conformation and interaction mode of the *rShPI-1/K13L* primary binding loop is not affected following the canonical mechanism usually reported for similar complexes with trypsin- and chymotrypsin-like enzymes (32–35). Most of the interactions are established by Leu¹⁵ at the P1 site, including the H-bonds typical for a substrate-like inhibition mechanism, and other contacts with aliphatic enzyme residues (Thr²¹³ and Val²¹⁶) that define the specificity for PPE. As expected, the hydrophobicity increase at the P1 side chain is accompanied by a moderate optimization of chymotrypsin inhibition by *rShPI-1/K13L*. Because the S1 pocket of chymotrypsin is characterized by the highest hydrophobic nature of these serine proteases, the associated K_i value decreased to the values reported for an equivalent K15L exchange of BPTI against this enzyme (7.7×10^{-10} M (27)).

Despite the absence of a positively charged residue at P1, the *rShPI-1/K13L* variant is still active against trypsin. Only a 2-orders of magnitude increase in the associated K_i value was detected compared with that of the wild-type inhibitor. A more significant effect was provoked by the equivalent exchange in BPTI, with K_i values shifting by 7 orders of magnitude from 6×10^{-14} M for the wild-type molecule to 1.8×10^{-7} M for the K15L variant (27). Because the P1 interactions of BPTI and *rShPI-1A* in the S1 pocket of trypsin are highly similar (35), significant differences in the contribution of further interaction sites to the overall complex stability were strongly indicated. The impact of subsites other than P1 directly correlates with the fitting accuracy of the latter within its S1 enzyme binding pocket. The

weaker the interaction of the P1 residue, the more prominent is the contribution of other inhibitor residues to the enzyme binding (32). In this context, we recently reported on an important stabilizing role of Arg¹¹ at the P3 position in the ShPI-1-trypsin interface that is thus far unique within this inhibitor family (35). This remote contribution is suggested to compensate for the reduced P1 interactions of the *rShPI-1/K13L* variant more effectively than in the corresponding BPTI complex.

The *rShPI-1/K13L*·PPE structure reported here provides the first structure-based evidence for a comparable impact of Arg¹¹ (P3) in the interface stabilization of a BPTI-Kunitz-type inhibitor and an elastase. Consequently, previous mutagenesis studies that proposed a correlation of the P3 residue in BPTI with its inhibitory activity against elastases without any structural knowledge are confirmed (26, 30). Residues different than the native Pro¹³ at P3 position in BPTI have been suggested to induce a more favorable primary loop conformation to strengthen HNE binding without affecting the PPE interaction (26). Our structure shows that the side chain of Arg¹¹ mediates interactions with a region of PPE that is characterized by sequential and structural differences compared with HNE, particularly involving loop structures containing Val^{99A}, Thr¹⁷⁵, and Arg^{217A} (according to PPE topology). This result supports a potential role of the P3 interaction in the elastase selectivity of BPTI-Kunitz inhibitors. In this regard, mutagenesis studies involving the squash seed *Cucurbita maxima* trypsin inhibitor III (CMTI-III) have shown that inhibition of HNE, but not of PPE or other serine proteases, occurs even if a Gly residue is located at P1 position, likewise indicating an impact of interactions distant to the S1 site in interface stability and elastase selectivity (6).

Moreover, we have identified a more significant impact of the secondary binding loop in the interaction with PPE compared

Crystal Structure of ShPI-1/K13L in Complex with Elastase

with previous reports of corresponding trypsin and chymotrypsin complexes (32–35), again supporting previous mutagenesis studies now on a structural level. Three basic residues in the segment ³⁹RAKR⁴² of the BPTI secondary loop (equivalent to ³⁷GGNG⁴⁰ in ShPI-1) have been reported to affect the inhibition activity against HNE. Substitution of this sequence in a BPTI/K15V variant by the equivalent stretch from Bikunin domain 2 (³⁹MGNG⁴²) increases the inhibition of HNE, whereas its effect on PPE inhibition has not been investigated (30). The increased amount of Gly residues within this region closely mimics the corresponding secondary loop sequence of ShPI-1, which is strongly involved in PPE interface stabilization via H-bonds according to the structural evidence provided here.

In this study we obtained a high-affinity PPE inhibitor from the BPTI-Kunitz family by site-directed mutagenesis at the P1 position. The detailed investigation of the enzyme-inhibitor interactions confirmed the expected canonical mechanism with a more important role of the inhibitor secondary binding loop compared with other S1 family serine proteases with known structures. Our data show that the P3 residue of rShPI-1/K13L points into a PPE region with significant structural difference compared with HNE, which has been described to be involved in the selectivity of WAP inhibitors toward HNE or PPE. Consequently, residues at the secondary binding loop and at the P3 site of ShPI-1 represent interesting targets for site-specific mutagenesis to improve binding affinity and/or direct selectivity against elastase-like enzymes. Because ShPI-1 does not contain any residue that can be oxidized within the serine protease binding loops, it represents a suitable scaffold to be developed into a specific inhibitor that binds HNE with high affinity, which is urgently required.

Acknowledgments—We thank Dr. M. Mansur for providing the pMB301 vector and Dr. F. P. Chávez (University of Chile) for support during the first mutagenesis experiments, as well as Drs. G. Cobaleda and S. Bromsoms (Autonomous University of Barcelona) for support in intensity-fading MALDI-TOF and peptide mapping experiments. We also thank Dr. T. Pons (Spanish Center for Cancer Research) for helpful advice concerning structural superposition and analysis and Katrin Seelhorst for critical reading of the manuscript.

References

1. Debelle, L., and Tamburro, A. M. (1999) Elastin: molecular description and function. *Int. J. Biochem. Cell Biol.* **31**, 261–272
2. Büchler, M., Uhl, W., and Malfertheiner, P. (1987) *Elastase 1 in Acute Pancreatitis: Research and Clinical Management* (Beger, H. G., and Büchler, M. D., eds), pp. 110–117, Springer Berlin Heidelberg, Berlin
3. Ooyama, T., and Sakamoto H. (1995) Elastase in the prevention of arterial aging and the treatment of atherosclerosis. *Ciba Found. Symp.* **192**, 307–317
4. Shapiro, S. D. (1995) The pathogenesis of emphysema: the elastase:anti-elastase hypothesis 30 years later. *Proc. Assoc. Am. Physicians* **107**, 346–352
5. Korkmaz, B., Horwitz, M. S., Jenne, D. E., and Gauthier, F. (2010) Neutrophil elastase, proteinase 3, and cathepsin G as therapeutic targets in human diseases. *Pharmacol. Rev.* **62**, 726–759
6. McWhorter, C. A., Walkenhorst, W. F., Campbell, E. J., and Glover, G. I. (1989) Novel inhibitors of human-leukocyte elastase and cathepsin G: sequence variants of squash seed protease inhibitor with altered protease selectivity. *Biochemistry* **28**, 5708–5714
7. Chughtai, B., and O'Riordan, T. G. (2004) Potential role of inhibitors of neutrophil elastase in treating diseases of the airway. *J. Aerosol Med.* **17**, 289–298
8. Moroy, G., Alix, A. J., Sapi, J., Hornebeck, W., and Bourguet, E. (2012) Neutrophil elastase as a target in lung cancer. *Anticancer Agents Med. Chem.* **12**, 565–579
9. Sun, Z., and Yang, P. (2004) Role of imbalance between neutrophil elastase and alpha 1-antitrypsin in cancer development and progression. *Lancet Oncol.* **5**, 182–190
10. Lane, A. A., and Ley, T. J. (2003) Neutrophil elastase cleaves PML-RAR α and is important for the development of acute promyelocytic leukemia in mice. *Cell* **115**, 305–318
11. Bode, W., Meyer, E., Jr., and Powers, J. C. (1989) Human leukocyte and porcine pancreatic elastase X-ray crystal structures, mechanism, substrate specificity, and mechanism-based inhibitors. *Biochemistry* **28**, 1951–1963
12. Koizumi, M., Fujino, A., Fukushima, K., Kamimura, T., and Takimoto-Kamimura, M. (2008) Complex of human neutrophil elastase with 1/2SLPI. *J. Synchrotron Radiat.* **15**, 308–311
13. Bode, W., Wei, A. Z., Huber, R., Meyer, E., Travis, J., and Neumann, S. (1986) X-ray crystal structure of the complex of human leukocyte elastase (PMN elastase) and the third domain of the turkey ovomucoid inhibitor. *EMBO J.* **5**, 2453–2458
14. Tsunemi, M., Matsuura, Y., Sakakibara, S., and Katsube, Y. (1996) Crystal structure of an elastase-specific inhibitor elafin complexed with porcine pancreatic elastase determined at 1.9 Å resolution. *Biochemistry* **35**, 11570–11576
15. Huang, K., Strynadka, N. C., Bernard, V. D., Peanasky, R. J., and James, M. N. (1994) The molecular structure of the complex of *Ascaris* chymotrypsin/elastase inhibitor with porcine elastase. *Structure* **2**, 679–689
16. Aÿ, J., Hilpert, K., Krauss, N., Schneider-Mergener, J., and Höhne, W. (2003) Structure of a hybrid squash inhibitor in complex with porcine pancreatic elastase at 1.8 Å resolution. *Acta Crystallogr. D Biol. Crystallogr.* **59**, 247–254
17. Kunitz, M., and Northrop, J. H. (1936) Isolation from beef pancreas of crystalline trypsinogen, trypsin, a trypsin inhibitor, and an inhibitor-trypsin compound. *J. Gen. Physiol.* **19**, 991–1007
18. Ascenzi, P., Bocedi, A., Bolognesi, M., Spallarossa, A., Coletta, M., De Cristofaro, R., and Menegatti, E. (2003) The bovine basic pancreatic trypsin inhibitor (Kunitz inhibitor), a milestone protein. *Curr. Protein Pept. Sci.* **4**, 231–251
19. Krowarsch, D., Cierpicki, T., Jelen, F., and Otlewski, J. (2003) Canonical protein inhibitors of serine proteases. *Cell. Mol. Life Sci.* **60**, 2427–2444
20. Schechter, I., and Berger, A. (1967) On the size of the active site in proteases. I. Papain. *Biochem. Biophys. Res. Commun.* **27**, 157–162
21. Delfín, J., Martínez, I., Antuch, W., Morera, V., González, Y., Rodríguez, R., Márquez, M., Saroyán, A., Larionova, N., Díaz, J., Padrón, G., and Chávez, M. (1996) Purification, characterization and immobilization of proteinase inhibitors from *Stichodactyla helianthus*. *Toxicol.* **34**, 1367–1376
22. Sinha, S., Watorek, W., Karr, S., Giles, J., Bode, W., and Travis, J. (1987) Primary structure of human neutrophil elastase. *Proc. Natl. Acad. Sci. U.S.A.* **84**, 2228–2232
23. McBride, J. D., Freeman, H. N., and Leatherbarrow, R. J. (1999) Selection of human elastase inhibitors from a conformationally constrained combinatorial peptide library. *Eur. J. Biochem.* **266**, 403–412
24. González, Y., Pons, T., Gil, J., Besada, V., Alonso-del-Rivero, M., Tanaka, A. S., Araujo, M. S., and Chávez, M. A. (2007) Characterization and comparative 3D modeling of CmPI-II, a novel 'nonclassical' Kazal-type inhibitor from the marine snail *Cenchritis muricatus* (Mollusca). *Biol. Chem.* **388**, 1183–1194
25. Tschesche, H., Beckmann, J., Mehlich, A., Schnabel, E., Truscheit, E., and Wenzel, H. R. (1987) Semisynthetic engineering of proteinase inhibitor homologues. *Biochim. Biophys. Acta* **913**, 97–101
26. Kraunsoe, J. A., Claridge, T. D., and Lowe, G. (1996) Inhibition of human leukocyte and porcine pancreatic elastase by homologues of bovine pancreatic trypsin inhibitor. *Biochemistry* **35**, 9090–9096
27. Krowarsch, D., Dadlez, M., Buczek, O., Krokoszynska, I., Smalas, A. O., and Otlewski, J. (1999) Interscaffolding additivity: binding of P1 variants of bovine pancreatic trypsin inhibitor to four serine proteases. *J. Mol. Biol.* **289**, 175–186

28. Kiczak, L., Kasztura, M., Koscielska-Kasprzak, K., Dadlez, M., and Otlewski, J. (2001) Selection of potent chymotrypsin and elastase inhibitors from M13 phage library of basic pancreatic trypsin inhibitor (BPTI). *Biochim. Biophys. Acta* **1550**, 153–163
29. Li, W., Wang, B. E., Moran, P., Lipari, T., Ganesan, R., Corpuz, R., Ludlam, M. J., Gogineni, A., Koeppen, H., Bunting, S., Gao, W. Q., and Kirchhofer, D. (2009) Pegylated Kunitz domain inhibitor suppresses hepsin-mediated invasive tumor growth and metastasis. *Cancer Res.* **69**, 8395–8402
30. Ley, A. C., Guterman, S. K., Markland, W., Kent, R. B., Roberts, B. L., and Ladner, R. C. (2003) ITI-D1 Kunitz domain mutants as HNE inhibitors. U. S. Patent 003/0175919 A1, pp. 1–55
31. Salameh, M. A., Soares, A. S., Hockla, A., Radisky, D. C., and Radisky, E. S. (2011) The P2' residue is a key determinant of mesotrypsin specificity, engineering a high affinity inhibitor with anticancer activity. *Biochem. J.* **440**, 95–105
32. Scheidig, A. J., Hynes, T. R., Pelletier, L. A., Wells, J. A., and Kossiakoff, A. A. (1997) Crystal structures of bovine chymotrypsin and trypsin complexed to the inhibitor domain of Alzheimer's amyloid β -protein precursor (APPI) and basic trypsin inhibitor (BPTI): engineering of inhibitors with altered specificities. *Protein Sci.* **6**, 1806–1824
33. Schmidt, A. E., Chand, H. S., Cascio, D., Kisiel, W., and Bajaj, S. P. (2005) Crystal structure of Kunitz domain 1 (KD1) of tissue factor pathway inhibitor-2 in complex with trypsin. *J. Biol. Chem.* **280**, 27832–27838
34. Helland, R., Leiros, I., Berglund, G. I., Willassen, N. P., and Smalås, A. O. (1998) The crystal structure of anionic salmon trypsin in complex with bovine pancreatic trypsin inhibitor. *Eur. J. Biochem.* **256**, 317–324
35. García-Fernández, R., Pons, T., Perbandt, M., Valiente, P. A., Talavera, A., González-González, Y., Rehders, D., Chávez, M. A., Betzel, C., and Redecke, L. (2012) Structural insights into serine protease inhibition by a marine invertebrate BPTI Kunitz-type inhibitor. *J. Struct. Biol.* **180**, 271–279
36. Antuch, W., Berndt, K. D., Chávez, M. A., Delfín, J., and Wüthrich, K. (1993) The NMR solution structure of a Kunitz-type proteinase inhibitor from the sea anemone *Stichodactyla helianthus*. *Eur. J. Biochem.* **212**, 675–684
37. Gil, D., García-Fernández, R., Alonso-del-Rivero, M., Lamazares, E., Pérez, M., Varas, L., Díaz, J., Chávez, M. A., González-González, Y., and Mansur, M. (2011) Recombinant expression of ShPI-1A, a non-specific BPTI-Kunitz-type inhibitor, and its protection effect on proteolytic degradation of recombinant human miniprotinsulin expressed in *Pichia pastoris*. *FEBS Yeast Res.* **7**, 575–586
38. García-Fernández, R., Pons, T., Meyer, A., Perbandt, M., González-González, Y., Gil, D. F., Chávez, M. A., Betzel, C., and Redecke, L. (2012) Crystal structure of the recombinant BPTI-Kunitz-type inhibitor rShPI-1A from the marine invertebrate *Stichodactyla helianthus*. *Acta Crystallogr. F Struct. Biol. Commun.* **68**, 1289–1293
39. Laemmli, U. K. (1970) Cleavage of structural proteins during the assembly of the head of bacteriophage T4. *Nature* **227**, 680–685
40. Estell, D. A., Graycar, T. P., Miller, J. V., Powers, D. B., Wells, J. A., Burnier, J. P., and Ng, P. G. (1986) Probing steric and hydrophobic effects on enzyme-substrate interactions by protein engineering. *Science* **233**, 659–663
41. Erlanger, B. F., Kokowsky, N., and Cohen, E. (1961) Preparation and properties of two new chromogenic substrates of trypsin. *Arch. Biochem. Biophys.* **95**, 271–278
42. Nakajima, K., Powers, J. C., Ashe, B. M., and Zimmerman, M. (1979) Mapping the extended substrate binding site of cathepsin G and human leukocyte elastase: studies with peptide substrates related to the α 1-protease inhibitor reactive site. *J. Biol. Chem.* **254**, 4027–4032
43. DelMar, E. G., Largman, C., Brodrick, J. W., and Geokas, M. C. (1979) A sensitive new substrate for chymotrypsin. *Anal. Biochem.* **99**, 316–320
44. Chase, T., Jr., and Shaw, E. (1967) *p*-Nitrophenyl-*p*'-guanidinobenzoate HCl: a new active site titrant for trypsin. *Biochem. Biophys. Res. Commun.* **29**, 508–514
45. Copeland, R. A., Lombardo, D., Glannaras, J., and Decicco, C. P. (1995) Estimating K_i values for tight binding inhibitors from dose-response plots. *Bioorg. Med. Chem.* **5**, 1947–1952
46. Bieth, J. G. (1995) Theoretical and practical aspects of proteinase inhibition kinetics. *Methods Enzymol.* **248**, 59–84
47. Leatherbarrow, R. J. (2009) *GraFit Version 7*, Erithacus Software Ltd., Horley, United Kingdom
48. Yanes, O., Villanueva, J., Querol, E., and Aviles, F. X. (2007) Detection of non-covalent protein interactions by “intensity fading” MALDI-TOF mass spectrometry: applications to proteases and protease inhibitors. *Nat. Protoc.* **2**, 119–130
49. Gasteiger, E., Hoogland, C., Gattiker, A., Duvaud, S., Wilkins, M. R., Appel, R. D., and Bairoch, A. (2005) Protein identification and analysis tools on the ExPASy server, in *The Proteomics Protocols Handbook* (Walker, J. M., ed) pp. 571–607, Humana Press, New York
50. Collaborative Computational Project, Number 4 (1994) The CCP4 suite: programs for protein crystallography. *Acta Crystallogr. D Biol. Crystallogr.* **50**, 760–763
51. McCoy, A. J., Grosse-Kunstleve, R. W., Adams, P. D., Winn, M. D., Storoni, L. C., and Read, R. J. (2007) Phaser crystallographic software. *J. Appl. Crystallogr.* **40**, 658–674
52. Würtele, M., Hahn, M., Hilpert, K., and Höhne, W. (2000) Atomic resolution structure of native porcine pancreatic elastase at 1.1 Å. *Acta Crystallogr. D Biol. Crystallogr.* **56**, 520–523
53. Emsley, P., Lohkamp, B., Scott, W. G., and Cowtan, K. (2010) Features and development of Coot. *Acta Crystallogr. D Biol. Crystallogr.* **66**, 486–501
54. Adams, P. D., Afonine, P. V., Bunkóczi, G., Chen, V. B., Davis, I. W., Echols, N., Headd, J. J., Hung, L. W., Kapral, G. J., Grosse-Kunstleve, R. W., McCoy, A. J., Moriarty, N. W., Oeffner, R., Read, R. J., Richardson, D. C., Richardson, J. S., Terwilliger, T. C., and Zwart, P. H. (2010) PHENIX: a comprehensive Python-based system for macromolecular structure solution. *Acta Crystallogr. D Biol. Crystallogr.* **66**, 213–221
55. Lüthy, R., Bowie, J. U., and Eisenberg, D. (1992) Assessment of protein models with three-dimensional profiles. *Nature* **356**, 83–85
56. Chen, V. B., Arendall, W. B., 3rd, Headd, J. J., Keedy, D. A., Immormino, R. M., Kapral, G. J., Murray, L. W., Richardson, J. S., and Richardson, D. C. (2010) MolProbity: all-atom structure validation for macromolecular crystallography. *Acta Crystallogr. D Biol. Crystallogr.* **66**, 12–21
57. Krissinel, E., and Henrick, K. (2007) Inference of macromolecular assemblies from crystalline state. *J. Mol. Biol.* **372**, 774–797
58. Vriend, G. (1990) WHAT IF, a molecular modeling and drug design program. *J. Mol. Graph.* **8**, 52–56
59. Eyal, E., Gerzon, S., Potapov, V., Edelman, M., and Sobolev, V. (2005) The limit of accuracy of protein modeling: influence of crystal packing on protein structure. *J. Mol. Biol.* **351**, 431–442
60. DeLano, W. L. *The PyMOL Molecular Graphics System* (2002) DeLano Scientific, San Carlos, CA
61. Vedvick, T., Buckholz, R. G., Engel, M., Urcan, M., Kinney, J., Provow, S., Siegel, R. S., and Thill, G. P. (1991) High-level secretion of biologically active aprotinin from the yeast *Pichia pastoris*. *J. Ind. Microbiol.* **7**, 197–201
62. Kjeldsen, T., Brandt, J., Andersen, A. S., Egel-Mitani, M., Hach, M., Pettersson, A. F., and Vad, K. (1996) A removable spacer peptide in a α -factor-leader/insulin precursor fusion protein improves processing and concomitant yield of the insulin precursor in *Saccharomyces cerevisiae*. *Gene* **170**, 107–112
63. Peanasky, R. J., Bentz, Y., Paulson, B., Graham, D. L., and Babin, D. R. (1984) The iso-inhibitors of chymotrypsin/elastase from *Ascaris lumbricoides*: isolation by affinity chromatography and association with the enzymes. *Arch. Biochem. Biophys.* **232**, 127–134
64. Zani, M. L., Nobar, S. M., Lacour, S. A., Lemoine, S., Boudier, C., Bieth, J. G., and Moreau, T. (2004) Kinetics of the inhibition of neutrophil proteinases by recombinant elafin and pre-elafin (trappin-2) expressed in *Pichia pastoris*. *Eur. J. Biochem.* **271**, 2370–2378
65. Apostoluk, W., and Otlewski, J. (1998) Variability of the canonical loop conformations in serine proteinases inhibitors and other proteins. *Proteins Struct. Funct. Genet.* **32**, 459–474